

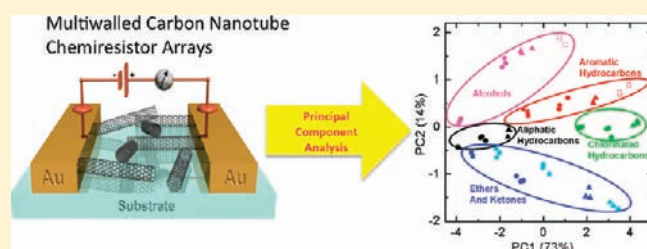
Diverse Chemiresistors Based upon Covalently Modified Multiwalled Carbon Nanotubes

Fei Wang and Timothy M. Swager*

Departments of Materials Science and Chemistry, Massachusetts Institute of Technology, Cambridge, Massachusetts 02139, United States

S Supporting Information

ABSTRACT: A diverse array of multiwalled carbon nanotube (MWCNT) sensory materials have been synthesized and used to create sensors capable of identifying volatile organic compounds (VOCs) on the basis of their functional groups. Functionalized MWCNTs with a series of cross-sensitive recognition groups were successfully synthesized via zwitterionic and post-transformation synthetic procedures. The incorporated chemical functional groups on MWCNT surfaces introduced greatly increased sensitivity and selectivity to the targeted analytes. The distinct response pattern of each chemical was subjected to statistical treatments, which led to a clear separation and accurate identification of 100% of the VOCs. These results demonstrate that covalently functionalized MWCNT-based sensor arrays are a promising approach for low-cost, real time detection and identification of VOCs.



INTRODUCTION

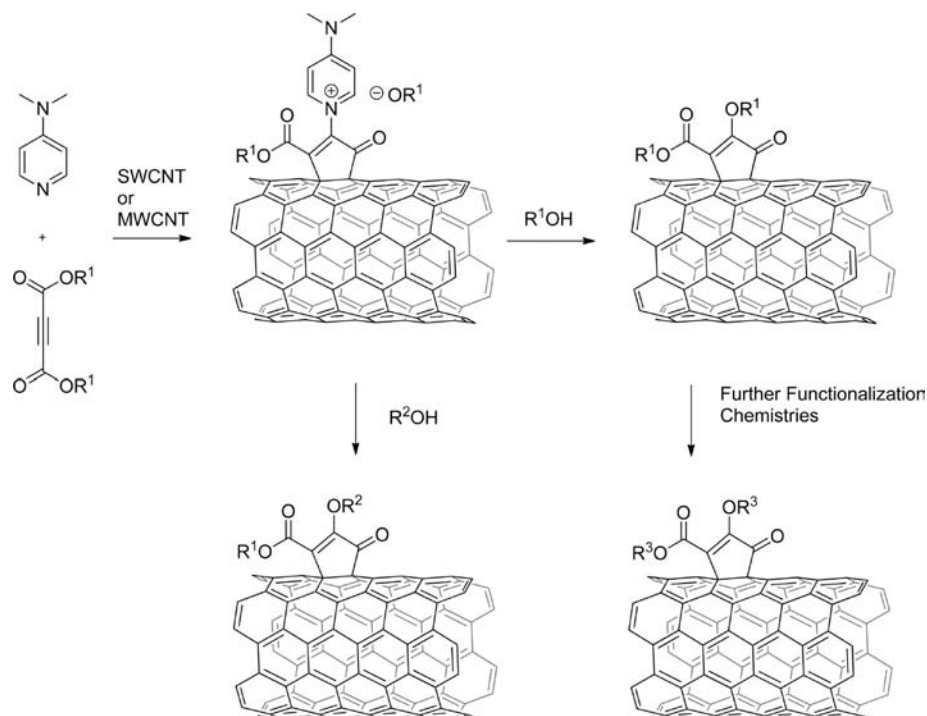
Real-time, sensitive detection and identification of volatile organic compounds are critically important to environmental monitoring and to human health. Widely used in many industries, many volatile organic chemicals (VOCs) can be toxic or carcinogenic even at relatively low concentrations. Additionally, VOCs in exhaled human breath have long been associated with certain diseases, and their detection and analysis have attracted a considerable amount of scientific interest.¹ For example, hydrocarbons detected in a patient's exhaled breath have been associated with cancer.^{2,3} Similarly, acetone is associated with uncontrolled diabetes,⁴ isoprene with cholesterol metabolism disorders,^{5,6} and sulfur-containing compounds with liver disfunctions.^{7,8} Breath analysis of exhaled VOCs have several obvious advantages over traditional diagnostic techniques. It is noninvasive, sampling less complex sample preparation than is required for blood or other body fluids, and has the potential for real-time monitoring. However, one of the major limitations preventing breath analysis from being used as a standard diagnostic technique is the lack of suitable and simple chemical detection and identification techniques.¹ Present clinical vapor analysis methods include gas chromatography–mass spectroscopy, solid-state metal oxide semiconductor sensors, and electrochemical methods, all of which require bulky and/or expensive instruments as well as considerable expertise to operate.⁹

Carbon nanotube (CNT) resistance-based chemical sensors have generated tremendous interest over the past decade.^{10–13} Chemiresistors have the advantages of low manufacturing cost, low power consumption, and minimal electronics. Additionally, resistance-based sensors can be easily miniaturized and thereby incorporated into other systems. Single-walled carbon nanotube

(SWCNT) sensors are recognized as ultrasensitive gas sensors, and have been studied for medical detection of organic vapors, including nonpolar molecules as cancer markers,^{14,15} carbon dioxide,¹⁶ and ethanol.¹⁷ The high sensitivity in SWCNT-based sensors is a result of the fact that their conductance dramatically responds to different chemical environments through charge transfer, charge carrier pinning, Schottky barrier changes, or CNT network swelling.^{10–13} A recent simulation study indicated that the sensing response of pristine nanotube networks is mainly induced by modulation of junction resistance, while the response of highly defective nanotube networks was mainly modulated by change in the nanotube resistance.¹⁸ As a result of the interest in maintaining high conductance, selectivity is generally introduced into SWCNT-based sensors through noncovalent modification as opposed to covalent sidewall functionalization. Specifically, disruptions in the π -system on the nanotube surface can give resistance increases by 3 orders of magnitude,¹⁹ and differential functionalization leads to large batch to batch variance in conductance and an increased background resistance that limits sensitivity. Although noncovalent functionalization methods can generate selectivity, they generally do not result in sensors that are sufficiently robust for harsh environment applications. With the goal of harnessing covalent modification of CNT sidewalls as a means to create a diverse array of robust sensors, we have decided to create chemiresistors having MWCNTs as the conductive element. The reasons for picking MWCNTs is that the dominance of the functionalization will be restricted to the outermost graphene wall and thereby the inner tubes will continue to be highly conductive. As

Received: March 1, 2011

Published: June 30, 2011

Scheme 1. Schematic Representation of the Reaction Schemes for Modular Functionalization of CNTs^a

^a For clarity, a SWCNT segment is shown with only a single added functional group.

as a result, we envision a chemiresistor where the MWCNT nanowires are made to have “functional insulation” about them and selective binding of analytes to the insulation will cause changes in the bulk conductance by modifying the internanotube resistance. In addition, polymer-carbon black conductive composites have also been widely explored for resistance based array sensing by swelling of the percolating network, and have achieved good sensitivity and selectivity.^{20,21} In these systems, the dispersion depends on the compatibility of carbon black and the polymer matrix, and melt-mixing followed by extrusion can be required to avoid excessive aggregation of carbon black.²² In contrast, our bottom-up approach uses surface modification of MWCNTs, and room temperature solution processes provide stable nanotube dispersions (“inks”) for device construction.

To install a range of surface bound functional groups, we have made use of a recently developed efficient modular functionalization method that can be applied to CNTs and fullerenes.^{23,24} The key reaction is initiated by a zwitterionic complex between 4-dimethylaminopyridine (DMAP) and disubstituted acetylenedicarboxylates (Scheme 1). The functionalization density can be as high as one incorporated functional group per nine carbons for SWCNTs and one per 38 carbons for multiwalled CNTs (MWCNTs). This approach allows for functionalization to create a diversity of sensory materials through modular nucleophilic substitution reactions of added alcohols with reactive pyridinium intermediates and transformations of reactive functional groups introduced by this method (Scheme 1).

In this contribution, we report a proof-of-concept sensing scheme using covalently functionalized MWCNTs to provide clear classification of VOCs based on functional group identification. We functionalized MWCNTs with a series of molecular recognition elements with differential binding abilities via zwitterionic functionalization and post-transformation synthetic

strategies. We demonstrate that the functionalized MWCNT sensor array has a dramatically enhanced sensing response to a variety of VOCs compared to pristine MWCNTs. The incorporation of molecular recognition elements has created a distinct response pattern for each of the chemicals investigated. Principal component analysis and linear discriminant analysis of the sensing data yielded a clear separation of the VOCs by their chemical families.

RESULTS

Design of the Sensor Array. The methodology for the array sensing is summarized in Figure 1. Initially, we observe the real time response of sidewall modified MWCNT sensor elements to selected VOCs. The obtained responses are then subjected to statistical treatments according to which analytes are then identified. Compared with individual sensors, array sensors have the advantages of responding to a wider range of analytes, improving selectivity, and identifying rather than only detecting a particular analyte.^{21,25} Array sensing using multiple receptors and pattern recognition process is very similar to the mammalian olfactory system and such devices have been referred to as “electronic noses” or “e-noses”.

Table 1 summarizes 20 VOCs selected as the test analytes. Each analyte has different chemical characteristics and different saturated vapor pressures. Unlike many highly reactive toxic gases which can be selectively detected on the basis of their strong chemical interactions such as Lewis acid–base, Brønsted acid–base or redox reactions, we chose to focus on VOCs that are relatively inert and are in principle more difficult to detect and identify.²⁶ As a proof of concept, we selectively detected them in order to demonstrate the advantages of incorporating diverse receptors/functionality in a sensor array.

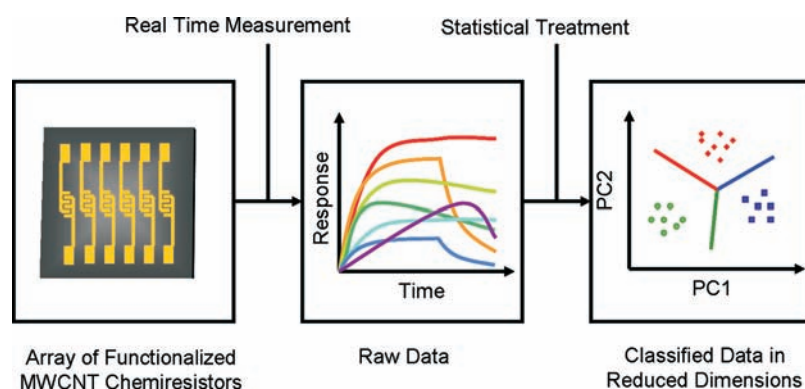


Figure 1. Outline of an array sensing process.

Table 1. Twenty Selected VOCs and Their Vapor Pressures^a at 298 K

analyte family/ functional group	analyte	vapor pressure	
		(mm Hg)	(ppm V)
Aliphatic Hydrocarbons	Dodecane	0.0977	128
	Decane	1.132	1489
	Octane	11.17	14697
Aromatic Hydrocarbons	1,3,5-Trimethylbenzene	0.9514	1251
	Xylenes	4.887	6430
	Toluene	22.35	29407
	Benzene	62	81578
Chlorinated Hydrocarbons	Chlorobenzene	9.774	12860
	1,2-Dichloroethane	60.9	80131
	Chloroform	152.9	201184
Ethers	Di- <i>n</i> -hexylether	0.06224	81
	Di- <i>n</i> -butylether	5.069	6669
	Dioxane	29.63	38986
Ketones	2-Decanone	0.269	353
	Cyclohexanone	2.766	3639
	Methylethylketone	68.88	90631
Alcohols	1-Octanol	0.06366	83
	1-Pentanol	1.545	2032
	1-Butanol	4.49	5907
	Ethanol	49.48	65105

^a Vapor pressures were obtained and calculated from *Yaws' Handbook of Antoine Coefficients for Vapor Pressure*,²⁷ or from the EPA's EPI software suite (<http://www.epa.gov/opptintr/exposure/docs/episuitedl.htm>) and should be taken as approximate only.

As detailed earlier, we chose MWCNTs as a chemiresistor material because, like SWCNTs, they can provide a rapid response to analytes, good reproducibility, and good reversibility. Additionally, the inner tubes in MWCNTs can maintain their electronic properties with high densities of covalent functionalization whereas similar modifications destroy the electronic structure of SWCNTs.²⁸ An additional issue with SWCNTs is their sensitivity to humidity changes.^{29,30}

The recognition groups in our sensor array are designed to provide a variety of noncovalent interactions with the VOCs' functional groups. Grate has developed a linear solvation energy relationship (LSER) approach to quantify the VOC sorption

with the contributing interactions.³¹ These interactions include hydrogen bonding, dipole–dipole interactions, polarizability, and hydrocarbon dispersion interactions. Figure 2 summarizes the strategic design of recognition groups according to these interactions and targeted analytes for each case. For hydrogen bonding, we have employed the hexafluoroisopropanol (HFIP) group which can maximize hydrogen bonding by its acidic hydroxyl group (pK_a 9–10, similar to phenols).^{32,33} We also included a carboxylic acid group in our sensors. Together, these two groups are targeted to hydrogen bond accepting vapors such as ethers and ketones. For hydrogen bonding basicity, we selected a readily available amide and crown-ether group, which provides high polarity and a preorganized basic site. This element is targeted to interact with hydroxyl-containing vapors such as alcohols and acids. The acetylenedicarboxylate ester adducts obtained from the initial zwitterionic functionalization are both polar and hydrogen bond accepting, and are thereby expected to interact strongly with vapors with large dipoles. Calix[4]arenes have a highly polarizable pocket which favors the adsorption of aromatic and chlorinated hydrocarbons. Long-chain dodecyl groups favor dispersion interactions (a balance between the exoergic process and the endoergic cost by entropy change) with aliphatic hydrocarbons.

Synthesis of Functionalized MWCNTs. The syntheses of sidewall functionalized MWCNTs are summarized in Schemes 2–5. Propargyl or allyl groups were initially introduced on to MWCNTs under mild zwitterionic reaction conditions (THF, 60 °C) by first reacting with dipropargyl or diallyl acetylenedicarboxylate and DMAP, followed by the respective addition of excess propargyl- or allyl-alcohol to yield propargyl-MWCNT **1** and allyl-MWCNT **2** (Scheme 2).^{23,24}

We have further functionalized **1** and **2** by three methods: 1,3-dipolar cycloaddition, thiol-ene addition, and olefin cross-metathesis reactions. The 1,3-dipolar cycloaddition and thiol-ene addition chemistry feature high yields and virtually no side products and are widely utilized to modify polymers, nanoscale materials, and biological materials.^{34,35} Olefin metathesis reactions, catalyzed by the Grubbs ruthenium catalysts, are another important route to introduce diversity, as these reactions generally proceed in good yields and with high functional group tolerance.^{36,37}

Using 1,3-dipolar cycloadditions, dodecyl groups were incorporated onto the propargyl-MWCNTs **1** by reaction with dodecyl azide with CuI and diisopropylethylamine (DIPEA) as catalysts (Scheme 3). Heating this reaction mixture in DMF at 90 °C for 24 h produced alkyltriazole-MWCNT **3** with pendant triazole groups.

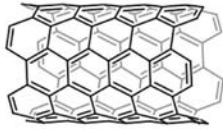
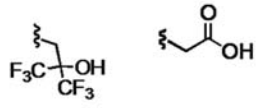
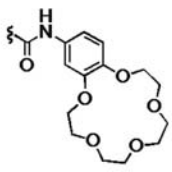
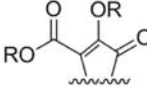
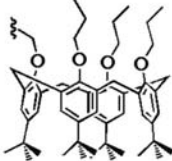
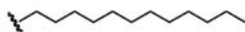
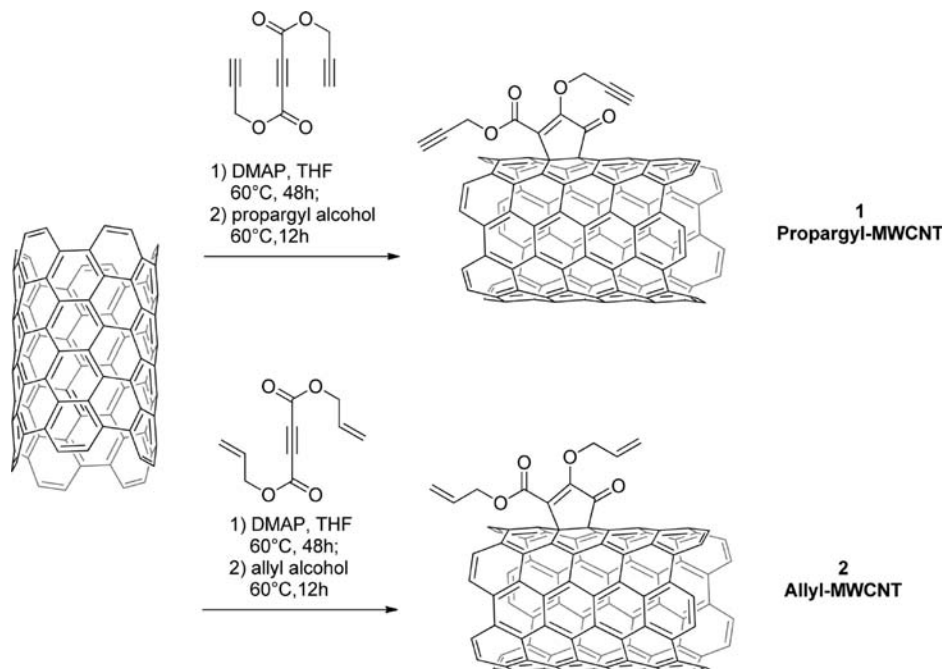
<p>MWCNT</p> 	<p>H-bond Acidity</p>  <p>Targeted Analytes: H-bond Acceptors such as Ethers, Ketones</p>	<p>H-bond Basicity</p>  <p>Targeted Analytes: H-bond Donors such as Acids, Alcohols</p>
<p>Polarity</p>  <p>R = allyl or propargyl</p> <p>Targeted Analytes: Vapors with High Polarity Such as Ketones, Ethers</p>	<p>Polarizability</p>  <p>Targeted Analytes: Aromatic and Chlorinated Hydrocarbons</p>	<p>Nonpolar Adsorption</p>  <p>Targeted Analytes: Aliphatic Hydrocarbons</p>

Figure 2. Selected recognition groups for differential interactions with targeted analytes.

Scheme 2. Synthesis of Propargyl-MWCNT 1 and Allyl-MWCNT 2^a

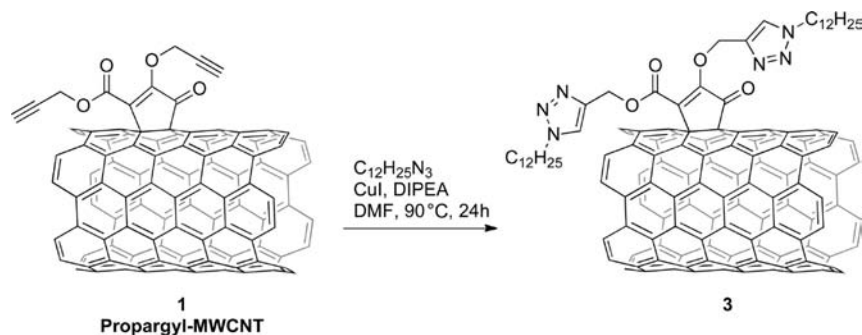


^a Note the MWCNTs are more complex polydisperse materials, and for clarity, a SWCNT segment is shown with only a single added functional group.

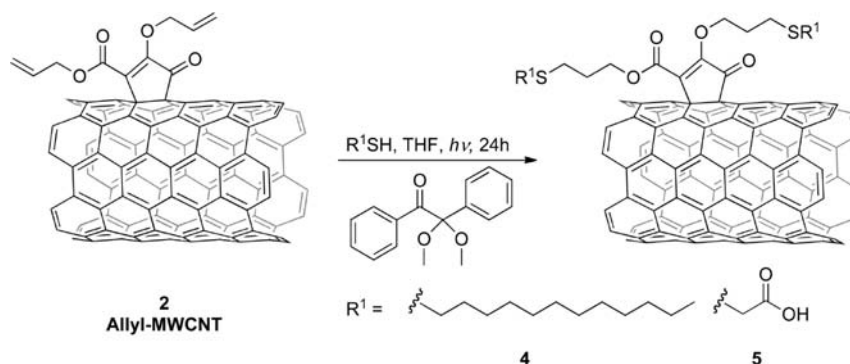
In the thiol-ene addition strategy, the vinyl group on allyl-MWCNT 2 was reacted with 1-dodecylthiol or thioglycolic acid under inert atmosphere with UV irradiation and 2,2-dimethoxy-2-phenylacetophenone as a photoinitiator (Scheme 4).^{35,38} These thiol-ene addition processes lead to the formation of

thiochain-MWCNT 4 with pendant dodecyl chains and thioacid-MWCNT 5 with pendant carboxylic acid groups.

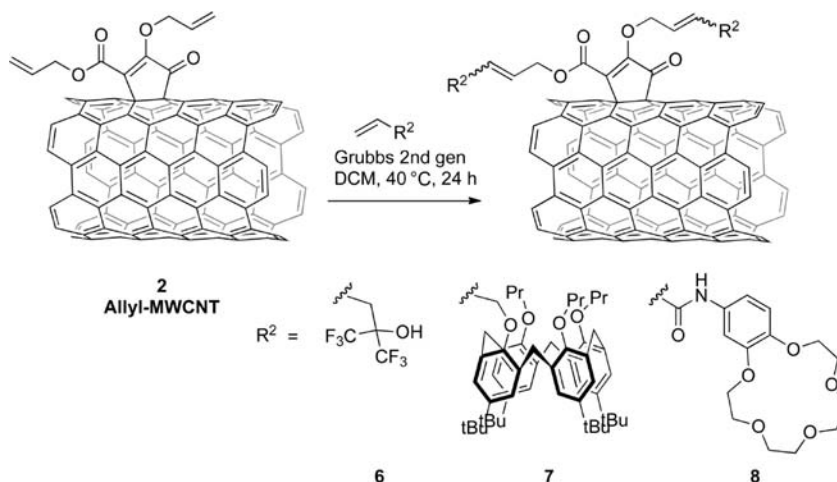
Cross-metathesis reactions were conducted between the allyl-MWCNT 3 and three terminal olefins; 2-allyl-hexafluoroisopropanol, allyl substituted calix[4]arene, and 4-acryloylamidobenzo-15-crown-5,

Scheme 3. Synthesis of Alkyltriazole-MWCNT 3^a

^a Note the MWCNTs are more complex polydisperse materials, and for clarity, a SWCNT segment is shown with only a single added functional group.

Scheme 4. Synthesis of Thiochain-MWCNT 4 and Thioacid-MWCNT 5^a

^a Note the MWCNTs are more complex polydisperse materials, and for clarity, a SWCNT segment is shown with only a single added functional group.

Scheme 5. Synthesis of HFIP-MWCNT 6, Calix-MWCNT 7, and Crown-MWCNT 8^a

^a Note the MWCNTs are more complex polydisperse materials, and for clarity, a SWCNT segment is shown with only a single added functional group.

using Grubbs second generation ruthenium catalyst,^{36,37} leading to HFIP-MWCNT 6, calix-MWCNT 7, and crown-MWCNT 8, respectively (Scheme 5).

Characterization. Previous transmission electron microscopy (TEM) studies have revealed that the functionalization does not result in gross structural changes of the CNTs.²⁴ The Raman spectra of pristine MWCNTs, propargyl-MWCNTs 1, and allyl-MWCNTs 2 are compared in Figure 3. Two characteristic bands

around 1330 cm^{-1} (D band) and 1580 cm^{-1} (G band) are immediately noticed. The D band reflects the structural disorder from defects or amorphous carbons, while the G band is associated with the tangential in-plane stretching vibration of the sp^2 carbon lattice. In contrast to SWCNTs, MWCNTs show an additional Raman band D' at around 1610 cm^{-1} , which is induced by disorder, defects, or ion intercalation between graphitic walls.^{39,40} The three spectra could be fit with two

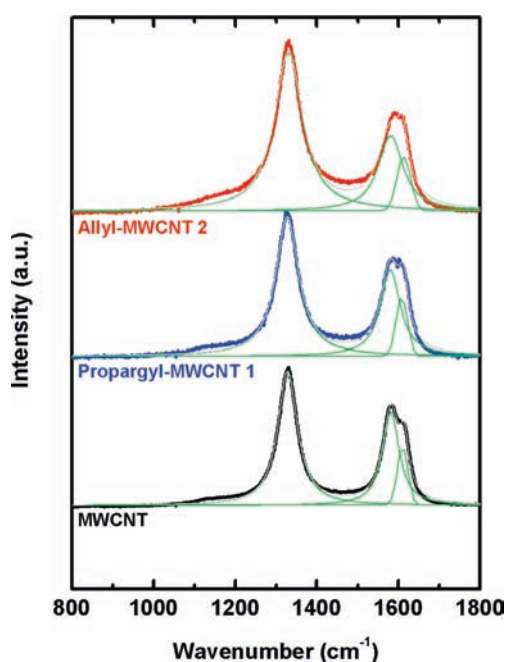


Figure 3. Raman spectra of pristine MWCNTs (black), propargyl-MWCNTs (blue), and allyl-MWCNTs (red). The green lines are fitted peaks and the gray lines are the fitted curves.

Lorentzian peaks for the D and G bands, and with a Gaussian peak for the D' band.^{41,42} The ratio of the intensity between D and G band increased from 1.7 for pristine MWCNTs to 1.9 and 2.3 for propargyl-MWCNTs 1 and allyl-MWCNTs 2, respectively; while the ratio of intensity between D' and G band remained the same (0.3) for all three samples. These results indicate that the zwitterionic functionalization reaction largely introduced covalent functionalization onto the MWCNT outermost graphene surface, with minimal perturbations to the inner tubes.

Although Raman spectroscopy gives evidence on the surface functionalization of nanotubes, Fourier transform infrared (FT-IR) spectroscopy reveals important chemical information regarding the incorporated functional groups.⁴³ As shown in Figure 4, all the functionalized MWCNTs have strong adsorption bands at 1730 cm^{-1} due to the C=O stretching of the carbonyl group and bands at 1230 and 1020 cm^{-1} assigned to the C–O stretching of the vinyl alkyl ether and ester groups. These features are consistent with the acetylenedicarboxylate diester adduct structure. All of the spectra of the functionalized MWCNTs were normalized according to the 1730 cm^{-1} peak.

The propargyl-MWCNT 1 displays three characteristic absorption bands at 3285, 2130, and 668 cm^{-1} , corresponding to the terminal $\equiv\text{C}-\text{H}$ stretching, the $\text{C}\equiv\text{C}$ stretching and the $-\text{C}\equiv\text{CH}$ bending of the propargyl group, respectively. After the 1,3-dipolar cycloaddition reaction, these three prominent bands completely disappear with concomitant enhanced peaks within the 3000–2800 cm^{-1} region as a result of the C–H stretching in the dodecyl groups, and a new peak appearing at 3130 cm^{-1} associated with the C–H stretching in the 1,2,3-triazole groups. This result indicates that the 1,3-dipolar cycloaddition reaction proceeded in high yield to produce 3.

Allyl-MWCNT 2 showed characteristic absorption bands of vinyl groups at 3087 and 921 cm^{-1} , corresponding to the $=\text{CH}_2$ stretching and the CH_2 out-of-plane wagging, respectively. After

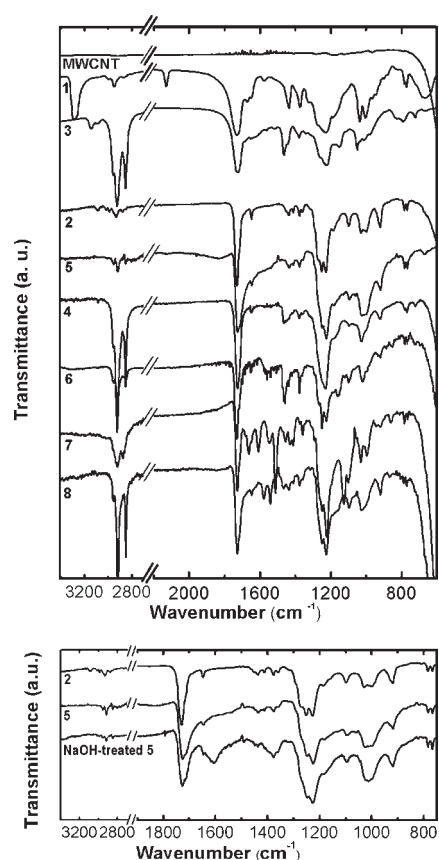


Figure 4. FT-IR spectroscopy of pristine and substituted MWCNTs (top): propargyl-MWCNT 1, allyl-MWCNT 2, alkytriazole-MWCNT 3, thiochain-MWCNT 4, thioacid-MWCNT 5, HFIP-MWCNT 6, calix-MWCNT 7, and crown-MWCNT 8. The spectra of thioacid-MWCNT treated with 0.1 M NaOH is also shown (bottom).

the thiol-ene addition, both bands of the allyl group had significantly decreased compared to the C=O stretching in the carbonyl group and the C–O stretching bands, indicating that the vinyl group has in large part undergone the proposed addition reaction. Importantly, the thioacid-MWCNT 5 became soluble in 0.1 M NaOH, and after base treatment displayed two new broad peaks at 1605 and 1376 cm^{-1} , which are associated with the asymmetric and symmetric stretching of the COO^- group, respectively (Figure 4, bottom). We also observed greatly enhanced absorption between 3000 and 2800 cm^{-1} for thiochain-MWCNTs 4, which are due to the C–H stretching in the dodecyl group. The large decrease of the vinyl absorption peaks and the appearance of the characteristic IR peaks of the new functional groups together verified the success of this thiol-ene addition modification.

Similar to the thiol-ene adducts, the MWCNTs from the metathesis reaction also showed significantly decreased IR absorption signals from the vinyl group along with the appearance of characteristic peaks of the new functional groups. Specifically, HFIP-MWCNT 6 showed a new peak at around 1170 cm^{-1} , corresponding to the C–F stretching in the HFIP group. The crown-MWCNT 8 showed a series of interesting bands: two peaks at 1660 and 1548 cm^{-1} due to the C=O stretching and C–O stretching in the amide group; three peaks at 1610, 1510, and 1456 cm^{-1} due to the aromatic ring stretching of the benzene ring; and a peak at 1125 cm^{-1} due to the

C–O–C three-centered stretching modes of the crown ether. The calix-MWCNT 7 showed the appearance of two new peaks at 1580 and 1542 cm^{-1} due to the aromatic ring stretching and a significant increase in the absorptions between 3000 and 2800 cm^{-1} due to the increased C–H stretching from the added *t*-butyl groups.

To obtain semiquantitative assessment of the degree of functionalization and composition of the modified MWCNTs, we have employed X-ray photoelectron spectroscopy (XPS) and thermogravimetric analysis (TGA). The XPS spectra (Figure 5) were normalized to the C 1s peak at 532 eV. In the TGA experiment (Figure 6), pristine MWCNTs cleaned in the same fashion as the functionalized MWCNTs were used as a standard. The weight loss data are obtained from subtracting the weight loss of the pristine MWCNTs.

Compared to pristine MWCNTs, both propargyl-MWCNTs 1 and allyl-MWCNTs 2 have increased intensity of oxygen 1s peak at 284 eV, indicating the success of the functionalization. From the oxygen-to-carbon ratio (7%), the calculated degree of functionalization density for propargyl-MWCNT 1 is 2 propargyl diester adduct groups per 100 MWCNT carbon atoms. This result agrees with the functionalization density of 2.0 functional

groups per 100 MWCNT carbon atoms calculated from the weight loss of 24% observed by TGA. Similar calculations were carried out for the allyl-MWCNTs 2, leading to a density of 3 allyl diester adduct groups per 100 MWCNT carbon atoms by XPS (oxygen-to-carbon ratio of 8%) and 2.6 functional groups by TGA (weight loss of 29%).

We observed a distinct nitrogen 1s peak at 400 eV in the alkyltriazole-MWCNT 3 sample, and calculated the functionalization density of the triazole group from the oxygen-to-carbon ratio (5%) or from the nitrogen-to-carbon ratio (6%). These ratios corresponded to 4 triazole groups per 100 MWCNT carbon atoms. The weight loss of 48% obtained from TGA measurements is in agreement and suggests functionalization density of 3.7 triazole groups per 100 carbon atoms. This high functionalization density indicated that the 1,3-dipolar cycloaddition chemistry is effectively quantitative on propargyl-MWCNTs 1, which was consistent with our FT-IR observations.

Important information on the elemental composition of other samples was also obtained from XPS. We noticed that the functionalization reaction led to quite different oxygen-to-nitrogen ratios in each sample. We also observed sulfur 2s and 2p peaks (at 229 and 165 eV, respectively) in thioacid-MWCNTs 5

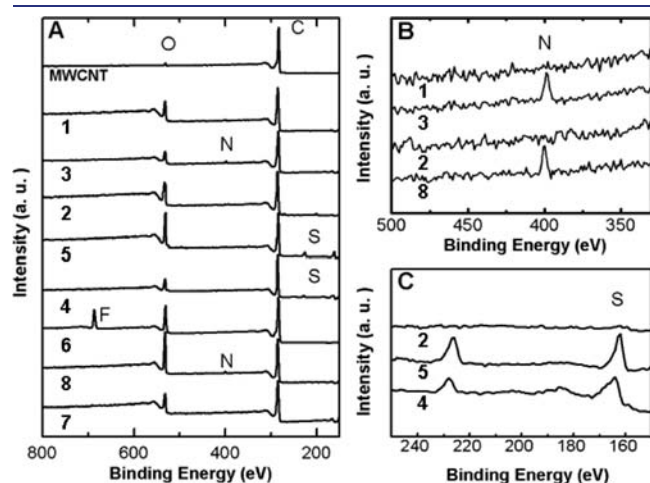


Figure 5. XPS of pristine and substituted MWCNTs: propargyl-MWCNT 1, allyl-MWCNT 2, alkyltriazole-MWCNT 3, thiochain-MWCNT 4, thioacid-MWCNT 5, HFIP-MWCNT 6, calix-MWCNT 7, and crown-MWCNT 8. (A) Broad scans showing relevant F, O, N and S peaks. (B) Expanded view of the N peaks. (C) Expanded view of the S peaks.

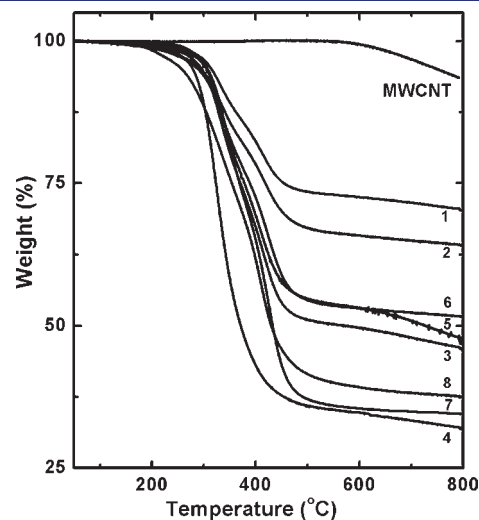


Figure 6. TGA of pristine and substituted MWCNTs: propargyl-MWCNT 1, allyl-MWCNT 2, alkyltriazole-MWCNT 3, thiochain-MWCNT 4, thioacid-MWCNT 5, HFIP-MWCNT 6, calix-MWCNT 7, and crown-MWCNT 8.

Table 2. Functionalization Density Data Calculated from the XPS Elemental Ratio and from the TGA Weight Loss Curves

samples	XPS elemental ratio (%)		TGA weight loss (%)	density (numbers of functional groups per 100 carbons)	
	O/C	X/C ^a		by XPS	by TGA
Propargyl-MWCNT	7	-	24	2	2.0
Allyl-MWCNT	8	-	39	3	2.6
Alkyltriazole-MWCNT	5	6	48	4	3.7
Thiochain-MWCNT	6	3	62	5	5.6
Thioacid-MWCNT	15	3	45	4	4.6
HFIP-MWCNT	12	7	42	2	1.6
Calix-MWCNT	8	-	59	- ^b	1.3
Crown-MWCNT	17	2	56	2	3.1

^aX stands for the respective amount of nitrogen, sulfur or fluorine in the samples. ^bXPS data is not used for calculation because functional group has similar oxygen-carbon ratio to parent allyl-MWCNT.

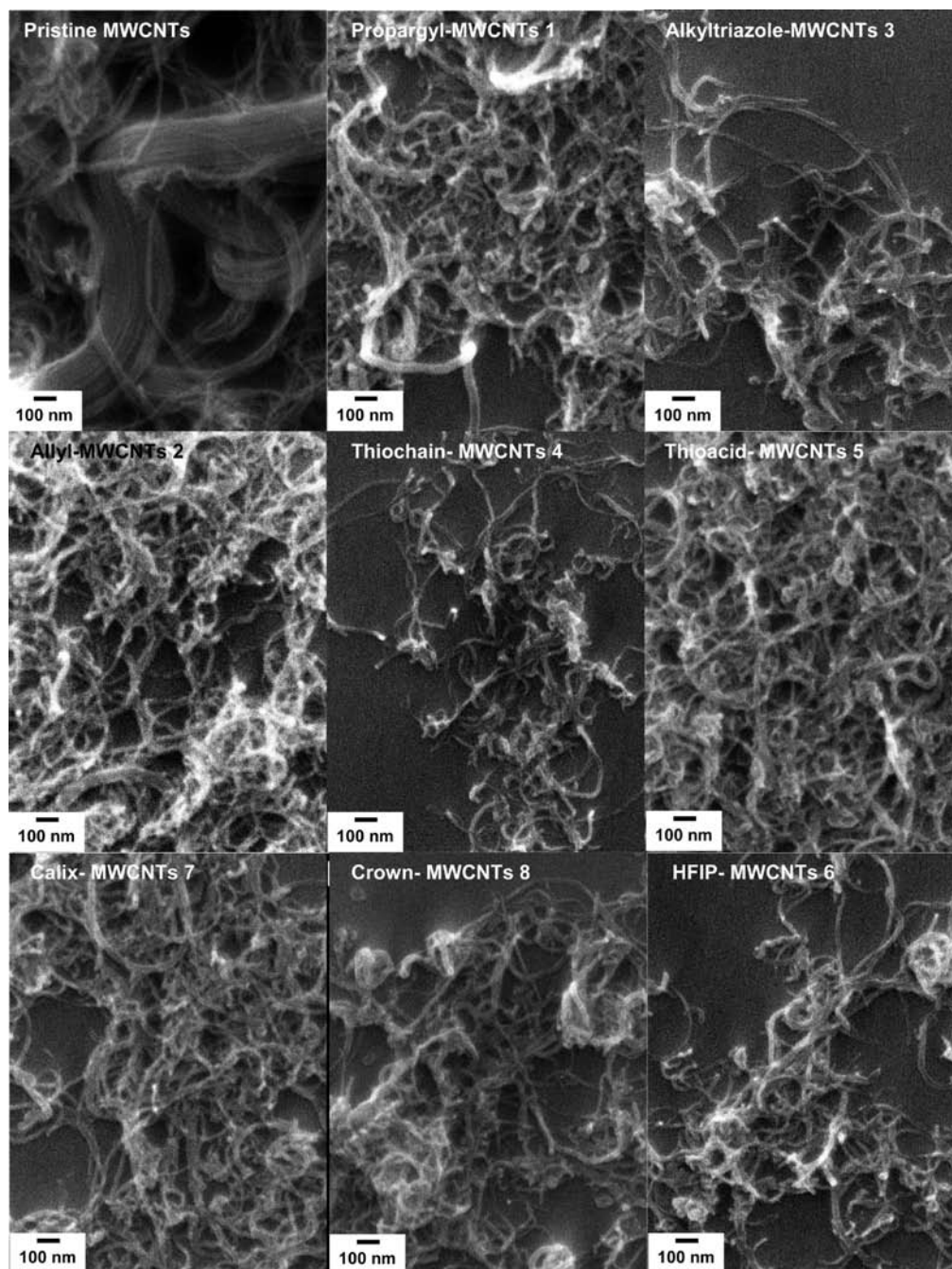


Figure 7. SEM images of pristine and substituted MWCNTs. The silicon substrates were cleaned by sonication in acetone/isopropyl alcohol/water successively and followed by cleaning with oxygen plasma for 3 min. MWCNT dispersions (0.1 mg/mL) were spin-coated on top of the substrates, and then annealed under vacuum at 150 °C for 5 min.

and thiochain-MWCNTs 4, a fluorine 1s peak at 687 eV in HFIP-MWCNTs 6, and a nitrogen 1s peak at 400 eV in crown-MWCNTs 8. Table 2 summarizes the functionalization density data calculated from the XPS elemental ratio and from the TGA curves.

Morphology and Dispersibility. The scanning electron microscope (SEM) images of functionalized MWCNTs are shown in Figure 7. As a comparison, pristine MWCNT were ultrasonicated and cleaned in the same fashion as the functionalized MWCNTs and were used as a standard, ruling out the effect of ultrasonication and solvent washing. Analysis of these

images confirmed that the functionalization process greatly reduced the size of the bundles of pristine MWCNTs.

Chemical treatment greatly enhanced the dispersibility of MWCNTs. For example, after centrifuging thiochain-MWCNT 4 suspension in dichloromethane at 14 500 rpm for 5 min, the vast majority of the material still remained in the supernatant layer. Untreated MWCNTs are quantitatively precipitated with similar treatment. This increase in dispersibility is not surprising, given the high density of long dodecyl chains (5.6 dodecyl groups per 100 MWCNT carbon atoms by TGA), and the debundled nature of the functionalized MWCNTs. Similar stable dispersibility

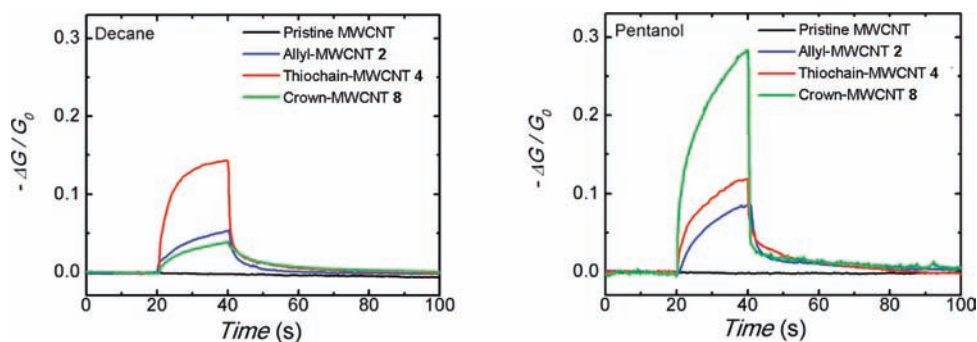


Figure 8. Conductance response, $-\Delta G/G_0$, of pristine MWCNTs (black line), allyl-MWCNTs 2 (dark red line), crown-MWCNTs 8 (green line), and thiochain-MWCNTs 4 (red line) resistance sensors to decane (left) and pentanol (right) at 1% of their saturated vapor pressures.

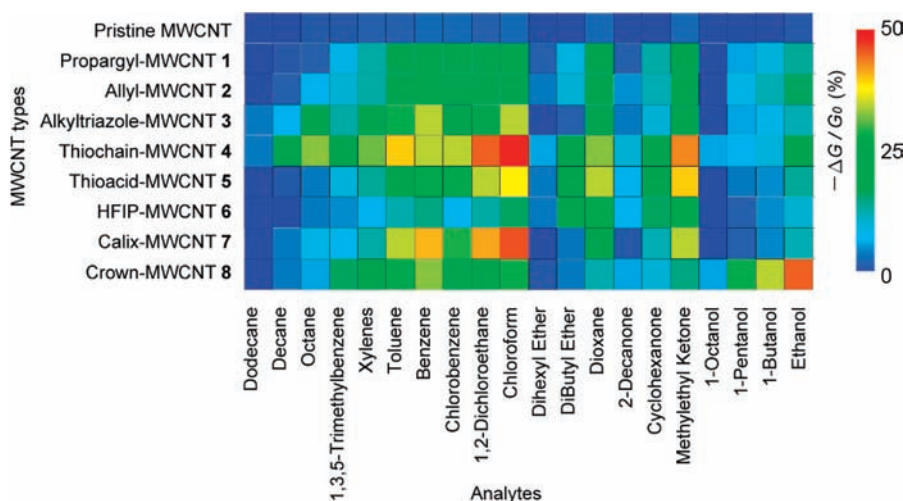


Figure 9. Conductance response patterns of pristine and substituted MWCNT based resistance sensors to 20 representative VOCs at 1% of their saturated vapor pressures. Responses are averages of three measurements. For easier visualization, the level of response is shown in color according to the scale bar on the right.

was also found with the HFIP-MWCNTs 6 and the thioacid-MWCNTs 5 in tetrahydrofuran, the crown-MWCNTs 8 in isopropyl alcohol, the calix-MWCNTs 7, and the alkyltriazole-MWCNTs 3 in dichloromethane. These good dispersion properties enable us to achieve high-quality CNT conductive networks, which are critical for sensor fabrication.

Sensory Responses of Functionalized MWCNTs to VOCs.

We fabricated our chemiresistors by spin coating dispersions (0.1 mg/mL) of functionalized MWCNTs onto 2 mm × 2 mm pairs of gold electrodes (50 nm thick, 2 mm spacing) on glass substrates. The solvents with the best dispersing ability, as mentioned in the Morphology and Dispersibility section, were used to create the solutions for spin coating of functionalized MWCNTs. Dimethylformamide was used for dispersing pristine, allyl- and propargyl-MWCNTs. The sensors were annealed after spin coating in vacuum at 150 °C for 5 min before obtaining measurements. The typical thickness of the MWCNT films was in the range of 30–60 nm measured with a profiler. The initial resistances for the MWCNT chemiresistors were in the range of 0.2 to 0.5 MΩ.

We investigated the sensory response by measuring the relative conductance change ($-\Delta G/G_0$) of the sensors upon exposure to the 20 VOCs at 1% of their saturated vapor pressures (3 trials each). The current was recorded between two electrodes

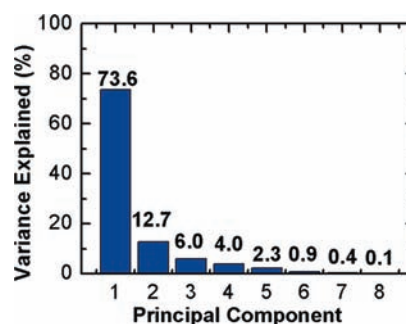


Figure 10. Scree plot of the principal component analysis.

under a constant bias voltage (0.05 V) from which the conductance change was calculated. Each sensor's response was measured sequentially under the same experimental conditions such as sensor exposure and refreshing time, analyte concentration, temperature, environmental humidity, and so forth.

Representative response curves of the sensor elements (pristine-MWCNTs, allyl-MWCNT 2, thiochain-MWCNTs 4, and crown-MWCNTs 8) to 1% saturated vapors of decane (left) and pentanol (right) are shown in Figure 8. All the sensors

responded to the analyte very rapidly and the chemical functionalization enhanced the response to both decane and pentanol. It is interesting that the conductance of the thiochain-MWCNTs 4 and the crown-MWCNTs 8 chemiresistors displayed complementary responses to decane and pentanol. This cross-sensitivity reflects the different chemical properties of the sensing elements. The long aliphatic hydrocarbon chains in the thiochain-MWCNTs lead to a stronger interaction with aliphatic hydrocarbons, and the amide and the crown ether groups in the crown-MWCNTs introduced favorable hydrogen bonding interactions with alcohol functionality of the pentanol.

Figure 9 is the conductance response matrix of pristine and substituted MWCNT based resistance sensors to 20 representative VOCs (1% of their saturated vapor pressure). Each response is the average of three measurements. For easier visualization, the level of response is shown in color according to the scale bar on the right. The responses to each analyte are summarized in Figure S1 (Supporting Information), with excellent device-to-device repeatability. As expected from our chosen functionality, each of the VOCs induced different conductance changes in the individual sensors, thereby creating a unique multidimensional response pattern. Compared with pristine MWCNTs, functionalized MWCNTs have dramatically enhanced responses to all the VOCs. This sensitivity is attributed to the enhanced absorption of analytes to the functionalized nanotube surface and the largely debundled CNT network. As opposed to SWCNTs,

MWCNTs have multiple graphenic layers and the electronic properties of the inner tubes are largely unaffected by surrounding chemical environment. The major mechanism of our MWCNT based sensor is, therefore, attributed to the adsorption of analytes onto the exterior surfaces of the MWCNT network and the subsequent change of the intertube (junction) resistance. This mechanism is similar to that of polymer/carbon-black network. The difference between this MWCNT network and carbon black network is that our MWCNT sensor is based on molecular level dispersion/modification of surfaces, while carbon black conductive network is based on macroscale dispersion.

Simple inspection of the data yields examples of the expected selectivity. For example, the HFIP-MWCNT 6 sensor has an increased response to ethers and ketones as a consequence of the high hydrogen bonding acidity of the HFIP group. More interestingly, the HFIP-MWCNT 6 sensor also showed a decreased response to all other VOCs. This latter property is attributed to the nonfavorable interactions between the HFIP's fluorocarbon groups and the hydrocarbon-containing VOCs. As a second example, the thiochain-MWCNT 4 sensor had a larger response to hydrocarbons with relatively low polarity such as aliphatic, aromatic, and chlorinated hydrocarbons. This is most likely due to the favorable dispersion interactions with the aliphatic recognition groups. Similar responses were observed for alkyltriazole-MWCNTs 3. We noticed the enhanced responses of thiochain-MWCNTs 4 to almost all of the VOCs, which is possibly due to its very high functionalization density (5.6 dodecyl groups per 100 MWCNT carbon atoms by TGA).

Statistical Analysis. To explore the capabilities of our sensor array to identify specific vapors, we subjected our sensing results to principal component analysis and linear discriminate analysis. Principal component analysis (PCA) is an unsupervised multivariate analysis method for linear data compression and pattern recognition.⁴⁴ Without any prior knowledge of the classification of the analytes, it groups the analytes based on the similarity of their data. The idea of PCA is to find uncorrelated principle components (PCs), which are linear combinations of the original variables (correlated response measurements). These PCs are ranked by the amount of variation they account for. As shown in the Scree plot (Figure 10), the PCA of our data set requires 2 PCs to describe 86% of the total variances and 4 PCs to describe 95% of the total variances. The PCA score plot in Figure 11 shows a clear classification of the data, utilizing the first two PCs, which represent 86% of the variances. The VOCs were classified into five groups, namely, alcohols, ethers/ketones, aliphatic, aromatic,

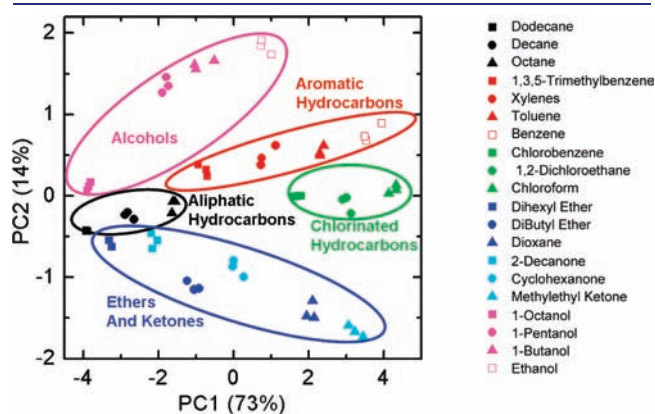


Figure 11. Principal component score plots of an array of 8 functionalized MWCNT resistance sensors to 20 representative VOCs (3 trials each).

Table 3. Summary of Classification with Cross-Validation

put-into-group	true group				
	chlorinated hydrocarbons	ethers/ketones	aliphatic hydrocarbons	alcohols	aromatic hydrocarbons
Chlorinated Hydrocarbons	9	0	0	0	0
Ethers/Ketones	0	18	0	0	0
Aliphatic Hydrocarbons	0	0	9	0	0
Alcohols	0	0	0	12	0
Aromatic Hydrocarbons	0	0	0	0	9
Total N	9	18	9	12	9
N Correct	9	18	9	12	9
Proportion	1.00	1.00	1.00	1.00	1.00

N = 60; N Correct = 60; Proportion Correct = 1.000

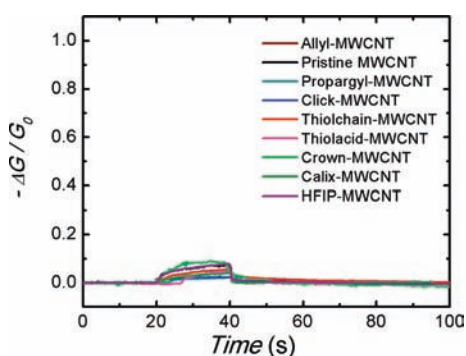


Figure 12. Conductance response, $-\Delta G/G_0$, of the pristine and substituted MWCNT based resistance sensors to saturated vapor of water.

and chlorinated hydrocarbons. The fact that both octanol and dihexyl ether have long aliphatic chains explains why their results also border the aliphatic hydrocarbon group. Although the ethers and the ketones are very clearly separated from other VOCs, it is difficult to distinguish them from each other because of their similar chemical properties.

We also explored the discrimination capability of our sensor with linear discriminant analysis (LDA).⁴⁴ LDA is a supervised statistical technique which utilizes data from known groups to identify which group a new object belongs to. It is based on the linear discriminant function (LDF), which is a linear combination of the original variables that maximizes the ratio of between-class variance and within-class variance. Specifically, we applied a cross-validation (leave-one-out) routine to compensate for an optimistic apparent error rate. This method calculates the LDF with one observation omitted sequentially and then classifies the omitted observation with the LDF. After this procedure is repeated for each observation, the success rate is calculated. In our case, the 60 training observations (20 VOCs, 3 trials for each) were separated into the same 5 groups utilized in the PCA classification. As shown in Table 3, the cross-validation routine LDA demonstrated 100% accuracy for all the 60 trials. This result, together with the successful PCA analysis, verified the excellent selectivity of our sensor array.

Humidity Response. Environmental humidity is always a concern for nanotube based sensors. As shown in Figure 12, our sensors have lower responses to humidity compared to their responses to organic molecules such as pentanol, although the saturated vapor pressure of water at 25 °C (23.8 mmHg) is 15 times larger than that of pentanol (1.5 mmHg). This fact can be explained by the hydrophobic nature of the incorporated chemical functionalizations. However, high humidity can potentially still generate relatively large responses when the MWCNTs are functionalized with strongly hydrogen bonding or Lewis acidic groups, or when the analyte concentration is very low. In these cases, humidity corrections may be needed.

CONCLUSIONS

Chemiresistor sensors capable of forming an array were developed from covalently sidewall functionalized MWCNTs for identifying VOCs. Functionalized MWCNTs with a series of cross-sensitive recognition groups were successfully synthesized via zwitterionic and post-transformation synthetic approaches. The incorporated chemical functional groups on MWCNT surfaces introduced greatly increased sensitivity and selectivity

to the targeted analytes. The covalent nature of the functionalization also yielded materials with excellent stability. The distinct response pattern of each chemical was subjected to statistical treatments, which led to a clear separation and accurate identification of 100% of the VOCs. MWCNT-based chemiresistive sensor arrays represent a promising approach for low-cost, real time detection and identification of VOCs.

EXPERIMENTAL SECTION

Materials. All chemicals were of reagent grade from Sigma-Aldrich, Alfa Aesar, or Acros and used as received. All solvents were of spectroscopic grade unless otherwise noted. Dimethylformamide was stirred over CaH_2 and distilled thereafter. Anhydrous tetrahydrofuran and dichloromethane were obtained from J. T. Baker and purified by passing through a Glasscontour dry solvent system. Multiwalled carbon nanotubes were acquired from Sigma-Aldrich. (>99 MWCNT, o.d. 6–13 nm \times 2.5–20 μm). Diallyl acetylenedicarboxylate and dipropargyl acetylenedicarboxylate were prepared according to literature procedures.²⁴ 5,11,17,23-Tetrakis(*t*-butyl)-25-allyl-26,27,28-tripropyl-calix[4]arene was prepared according to literature procedure.⁴⁵

General Methods and Instrumentation. Raman spectra were measured with a Kaiser Hololab 5000R Modular Research Raman Spectrometer with Microprobe from MIT Center for Materials Science and Engineering. FT-IR spectra were recorded on a Perkin-Elmer Model 2000 FT-IT spectrometer by drop-casting the material on a KBr disk. TGA analyses were performed with a TGA Q50 apparatus (TA Instruments). Experiments were carried out under nitrogen. Samples were heated at 5 °C/min from 30 to 800 °C. XPS spectra were recorded on a Kratos AXIS Ultra X-ray Photoelectron Spectrometer. SEM images were taken with a JEOL 6700 Scanning Electron Microscope. Gold layer was coated from a Polaron SC7620 sputter coater. The substrates were cleaned with a Harrick Plasma PDC-32G Plasma Cleaner. Film thicknesses were measured with a Veeco Dektak 6 M Stylus Profiler.

All synthetic manipulations were carried out under an argon atmosphere using standard Schlenk techniques unless otherwise noted. Glassware was oven-baked and cooled under N_2 atmosphere. Analyte of specific concentration and relative humidity was generated with a KIN-TEK gas-generating system. Source-drain current change in response to analyte was measured with an AUTOLAB PGSTAT 20 potentiostat (Eco Chemie) at constant potential (typically 0.05 V). The statistical treatment was performed with a Minitab software (version 15) using multivariate analysis methods.

Synthesis of Propargyl-MWCNTs 1. A suspension of MWCNTs (48.0 mg, 4.0 mmol of carbon) in THF (40 mL) was sonicated for 5 min using an ultrasonic probe yielding a black suspension. To the MWCNT suspension were added activated molecular sieves (4 Å) to remove moisture introduced by the sonication process, and left overnight. The heterogeneous solution was then transferred to a dry flask through a cannula and was heated at 60 °C. To the MWCNT suspension were added simultaneously a solution of dipropargyl acetylenedicarboxylate (3.80 g, 20.0 mmol) in THF (20 mL) and a solution of 4-dimethylaminopyridine (2.44 g, 20.0 mmol) in THF (20 mL) via syringe pump over 48 h. Propargyl alcohol (1.5 mL) was then added and the resulting mixture was stirred at 60 °C for another 12 h. The reaction mixture was cooled to room temperature and centrifuged at 14 500 rpm for 15 min. The supernatant was discarded and the residue was dispersed in DMF for 3 min using an ultrasonic bath. The mixture was centrifuged and the supernatant was discarded. The same dispersion, centrifugation, and supernatant separation sequence was repeated five times with DMF and five times with acetone to remove impurities. The propargyl-MWCNTs 1 were dried under vacuum overnight. See Figure 3 for Raman spectra, Figure 4 for FT-IR spectra, Figure 5 for XPS spectra, Figure 6 for TGA weight loss curve, and Figure 7 for SEM image.

Synthesis of Allyl-MWCNTs 2. A suspension of MWCNTs (48.0 mg, 4.0 mmol of carbon) in THF (40 mL) was sonicated for 5 min using an ultrasonic probe yielding a black suspension. To the MWCNT suspension were added activated molecular sieves (4 Å) to remove moisture introduced by the sonication process, and left overnight. The heterogeneous solution was then transferred to a dry flask through a cannula and was heated at 60 °C. To the MWCNT suspension were added simultaneously a solution of diallyl acetylenedicarboxylate (3.88 g, 20.0 mmol) in THF (20 mL) and a solution of 4-dimethylaminopyridine (2.44 g, 20.0 mmol) in THF (20 mL) via syringe pump over 48 h. Allyl alcohol (1.5 mL) was then added, and the resulting mixture was stirred at 60 °C for another 12 h. The reaction mixture was cooled to room temperature and centrifuged at 14 500 rpm for 15 min. The supernatant was discarded and the residue was dispersed in DMF for 3 min using an ultrasonic bath. The mixture was centrifuged and the supernatant was discarded. The same dispersion, centrifugation, and supernatant separation sequence was repeated five times with DMF and five times with acetone to remove impurities. The allyl-MWCNTs 2 were dried under vacuum overnight. See Figure 4 for FT-IR spectra, Figure 5 for XPS spectra, Figure 6 for TGA weight loss curve, and Figure 7 for SEM image.

Synthesis of Alkyltriazole-MWCNTs 3. To a 10 mL Schlenk flask was added propargyl-MWCNTs 1 (10 mg) and CuI (38 mg, 0.2 mmol), followed by sequentially vacuuming and refilling with argon three times. Then dodecyl azide (0.22 g, 1 mmol), diisopropylethylamine (2 mL), and dimethylformamide (2 mL) were added via syringe. The mixture was sonicated in a sonication bath for 30 min, followed by stirring at 90 °C for 24 h. The reaction mixture was cooled to room temperature and washed with ammonium hydroxide for five times to remove copper. Interestingly, the MWCNTs were well dispersed in the diisopropylethylamine phase during the washing process, so a 25 mL separation funnel was used to collect the diisopropylethylamine phase. The dispersion was further washed with water three times to remove residue ammonium hydroxide. The dispersion was added to methanol and centrifuged at 14 500 rpm for 15 min. The supernatant was discarded and the residue was dispersed in acetone for 3 min using an ultrasonic bath. The mixture was centrifuged and the supernatant was discarded. The same dispersion, centrifugation, and supernatant separation sequence was repeated five times with acetone to remove impurities. The alkyltriazole-MWCNTs 3 were dried under vacuum overnight. See Figure 3 for Raman spectra, Figure 4 for FT-IR spectra, Figure 5 for XPS spectra, Figure 6 for TGA weight loss curve, and Figure 7 for SEM image.

Synthesis of Thiochain-MWCNTs 4. To a 10 mL Schlenk flask was added allyl-MWCNTs 2 (10 mg) and 2,2-dimethoxy-2-phenylacetophenone (DMPA) (26 mg, 0.1 mmol), followed by sequentially vacuuming and refilling with argon three times. Then, *n*-dodecylthiol (0.40 g, 2 mmol) and tetrahydrofuran (2 mL) were added via syringe. The mixture was sonicated in a sonication bath for 30 min, followed by stirring under UV irradiation at room temperature for 24 h. The reaction mixture was then diluted with acetone and centrifuged at 14 500 rpm for 15 min. The supernatant was discarded and the residue was dispersed in acetone for 3 min using an ultrasonic bath. The mixture was centrifuged and the supernatant was discarded. The same dispersion, centrifugation, and supernatant separation sequence was repeated five times with acetone to remove impurities. The thiochain-MWCNTs 4 were dried under vacuum overnight. See Figure 4 for FT-IR spectra, Figure 5 for XPS spectra, Figure 6 for TGA weight loss curve, and Figure 7 for SEM image.

Synthesis of Thioacid-MWCNTs 5. To a 10 mL Schlenk flask was added allyl-MWCNTs 2 (10 mg) and 2,2-dimethoxy-2-phenylacetophenone (DMPA) (26 mg, 0.1 mmol), followed by sequentially vacuuming and refilling with argon three times. Then thioglycolic acid (0.18 g, 2 mmol) and tetrahydrofuran (2 mL) were added via syringe. The mixture was sonicated in a sonication bath for 30 min, followed by

stirring under UV irradiation at room temperature for 24 h. The reaction mixture was then diluted with acetone and centrifuged at 14 500 rpm for 15 min. The supernatant was discarded and the residue was dispersed in acetone for 3 min using an ultrasonic bath. The mixture was centrifuged and the supernatant was discarded. The same dispersion, centrifugation, and supernatant separation sequence was repeated five times with acetone to remove impurities. The thioacid-MWCNTs 5 were dried under vacuum overnight. See Figure 4 for FT-IR spectra, Figure 5 for XPS spectra, Figure 6 for TGA weight loss curve, and Figure 7 for SEM image.

Synthesis of HFIP-MWCNTs 6. To a 10 mL Schlenk flask was added allyl-MWCNTs 2 (10 mg) and Grubbs second generation ruthenium catalyst (8 mg, 0.01 mmol), followed by sequentially evacuating and refilling with argon three times. Then, 2-allyl-hexafluoroisopropanol (0.4 g, 2 mmol) and dichloromethane (2 mL) were added via syringe. The mixture was sonicated in a sonication bath for 30 min, followed by stirring at 40 °C for 48 h. The reaction mixture was then diluted with acetone and centrifuged at 14 500 rpm for 15 min. The supernatant was discarded and the residue was dispersed in acetone for 3 min using an ultrasonic bath. The mixture was centrifuged and the supernatant was discarded. The same dispersion, centrifugation, and supernatant separation sequence was repeated five times with acetone to remove impurities. The HFIP-MWCNTs 6 were dried under vacuum overnight. See Figure 4 for FT-IR spectra, Figure 5 for XPS spectra, Figure 6 for TGA weight loss curve, and Figure 7 for SEM image.

Synthesis of Calix-MWCNTs 7. To a 10 mL Schlenk flask was added allyl-MWCNTs 2 (10 mg), Grubbs second generation ruthenium catalyst (8 mg, 0.01 mmol), and 5,11,17,23-tetrakis(*t*-butyl)-25-allyl-26,27,28-tripropyl-calix[4]arene (0.16 g, 0.2 mmol) followed by sequentially evacuating and refilling with argon three times. Then dichloromethane (2 mL) was added via syringe. The mixture was sonicated in a sonication bath for 30 min, followed by stirring at 40 °C for 48 h. The reaction mixture was then diluted with acetone and centrifuged at 14 500 rpm for 15 min. The supernatant was discarded and the residue was dispersed in acetone for 3 min using an ultrasonic bath. The mixture was centrifuged and the supernatant was discarded. The same dispersion, centrifugation, and supernatant separation sequence was repeated five times with acetone to remove impurities. The calix-MWCNTs 7 were dried under vacuum overnight. See Figure 4 for FT-IR spectra, Figure 5 for XPS spectra, Figure 6 for TGA weight loss curve, and Figure 7 for SEM image.

Synthesis of Crown-MWCNTs 8. To a 10 mL Schlenk flask was added allyl-MWCNTs 2 (10 mg), Grubbs second generation ruthenium catalyst (8 mg, 0.01 mmol), and 4-acryloylamidobenzo-15-crown-5 (0.14 g, 0.4 mmol) followed by sequentially evacuating and refilling with argon three times. Then, dichloromethane (2 mL) was added via syringe. The mixture was sonicated in a sonication bath for 30 min, followed by stirring at 40 °C for 48 h. The reaction mixture was then diluted with acetone and centrifuged at 14 500 rpm for 15 min. The supernatant was discarded and the residue was dispersed in acetone for 3 min using an ultrasonic bath. The mixture was centrifuged and the supernatant was discarded. The same dispersion, centrifugation, and supernatant separation sequence was repeated five times with acetone to remove impurities. The crown-MWCNTs 8 were dried under vacuum overnight. See Figure 4 for FT-IR spectra, Figure 5 for XPS spectra, Figure 6 for TGA weight loss curve, and Figure 7 for SEM image.

Device Fabrication. The glass substrates were cleaned by sonication in acetone/isopropyl alcohol/water successively and followed by cleaning with oxygen plasma for 5 min. Two gold strip electrodes (50 nm thick, 2 mm spacing) were sputter-coated, and MWCNT dispersions were spin-coated on top of the gold electrodes. The devices were then annealed under vacuum at 150 °C for 5 min. The typical thickness of the MWCNT films is in the range of 30–60 nm measured with a profiler. The typical resistance for the MWCNT films is in the range of 0.2–0.5 MΩ.

Device Measurement. We investigated the sensory response by measuring the relative conductance change ($-\Delta G/G_0$) of the sensors upon exposure to the 20 VOCs (3 trials each). The current was recorded between the two electrodes under a constant bias voltage (0.05 V) from which the conductance change was calculated. Our sensor response is taken one at a time, under the same experimental conditions such as sensor exposure and refreshing time, analyte concentration, temperature, environmental humidity, and so forth.

■ ASSOCIATED CONTENT

S Supporting Information. Conductance response of pristine and substituted MWCNT based resistance sensors to 20 representative VOCs. This material is available free of charge via the Internet at <http://pubs.acs.org>.

■ AUTHOR INFORMATION

Corresponding Author

tswager@mit.edu

■ ACKNOWLEDGMENT

We are grateful for support from the National Science Foundation and the Army Research Office through the Institute for Soldier Nanotechnologies.

■ REFERENCES

- (1) Buszewski, B.; Kesy, M.; Ligor, T.; Amann, A. *Biomed. Chromatogr.* **2007**, *21*, 553–566.
- (2) O'Neill, H. J.; Gordon, S. M.; O'Neill, M. H.; Gibbons, R. D.; Szidon, J. P. *Clin. Chem* **1988**, *34*, 1613–1618.
- (3) Phillips, M.; Gleeson, K.; Hughes, J. M. B.; Greenberg, J.; Cataneo, R. N.; Baker, L.; McVay, W. P. *Lancet* **1999**, *353*, 1930–1933.
- (4) Deng, C.; Zhang, J.; Yu, X.; Zhang, W.; Zhang, X. *J. Chromatogr., B* **2004**, *810*, 269–275.
- (5) Miekisch, W.; Schubert, J. K.; Noeldge-Schomburg, G. F. E. *Clin. Chim. Acta* **2004**, *347*, 25–39.
- (6) Stone, B.; Besse, T.; Duane, W.; Dean Evans, C.; DeMaster, E. *Lipids* **1993**, *28*, 705–708.
- (7) Di Francesco, F.; Fuoco, R.; Trivella, M.; Ceccarini, A. *Microchem. J.* **2005**, *79*, 405–410.
- (8) Libardoni, M.; Stevens, P.; Waite, J. H.; Sacks, R. *J. Chromatogr., B* **2006**, *842*, 13–21.
- (9) Amann, A.; Smith, D. *Breath Analysis for Clinical Diagnosis and Therapeutic Monitoring*; World Scientific Publishing Company: London, 2005.
- (10) Allen, B. L.; Kichambare, P.; Star, A. *Adv. Mater.* **2007**, *19*, 1439–1451.
- (11) Kauffman, D. R.; Star, A. *Angew. Chem., Int. Ed.* **2008**, *47*, 6550–6570.
- (12) Kim, S. N.; Rusling, J.; Papadimitrakopoulos, F. *Adv. Mater.* **2007**, *19*, 3214–3228.
- (13) Snow, E. S.; Perkins, F. K.; Robinson, J. A. *Chem. Soc. Rev.* **2006**, *35*, 790–798.
- (14) Peng, G.; Trock, E.; Haick, H. *Nano Lett.* **2008**, *8*, 3631–3635.
- (15) Peng, G.; Tisch, U.; Haick, H. *Nano Lett.* **2009**, *9*, 1362–1368.
- (16) Star, A.; Han, T.; Joshi, V.; Gabriel, J.; Grüner, G. *Adv. Mater.* **2004**, *16*, 2049–2052.
- (17) Someya, T.; Small, J.; Kim, P.; Nuckolls, C.; Yardley, J. T. *Nano Lett.* **2003**, *3*, 877–881.
- (18) Salehi-Khojin, A.; Khalili-Araghi, F.; Kuroda, M. A.; Lin, K. Y.; Leburton, J.; Masel, R. I. *ACS Nano* **2011**, *5*, 153–158.
- (19) Gomez-Navarro, C.; Pablo, P. J. D.; Gomez-Herrero, J.; Biel, B.; Garcia-Vidal, F. J.; Rubio, A.; Flores, F. *Nat. Mater.* **2005**, *4*, 534–539.
- (20) Muñoz, B. C.; Steintal, G.; Sunshine, S. *Sens. Rev.* **1999**, *19*, 300–305.
- (21) Lonergan, M. C.; Severin, E. J.; Doleman, B. J.; Beaber, S. A.; Grubbs, R. H.; Lewis, N. S. *Chem. Mater.* **1996**, *8*, 2298–2312.
- (22) Huang, J. *Adv. Polym. Technol.* **2002**, *21*, 299–313.
- (23) Zhang, W.; Swager, T. M. *J. Am. Chem. Soc.* **2007**, *129*, 7714–7715.
- (24) Zhang, W.; Sprafke, J. K.; Ma, M.; Tsui, E. Y.; Sydlík, S. A.; Rutledge, G. C.; Swager, T. M. *J. Am. Chem. Soc.* **2009**, *131*, 8446–8454.
- (25) Albert, K. J.; Lewis, N. S.; Schauer, C. L.; Sotzing, G. A.; Stitzel, S. E.; Vaid, T. P.; Walt, D. R. *Chem. Rev.* **2000**, *100*, 2595–2626.
- (26) Lim, S. H.; Feng, L.; Kemling, J. W.; Musto, C. J.; Suslick, K. S. *Nat. Chem.* **2009**, *1*, 562–567.
- (27) Yaws, C. L. *Yaws Handbook of Vapor Pressure: Antoine Coefficients*; Gulf Publishing Company: Houston, TX, 2007.
- (28) Balasubramanian, K.; Burghard, M. *Small* **2005**, *1*, 180–192.
- (29) Kim, W.; Javey, A.; Vermesh, O.; Wang, Q.; Li, Y.; Dai, H. *Nano Lett.* **2003**, *3*, 193–198.
- (30) Zahab, A.; Spina, L.; Poncharal, P.; Marlière, C. *Phys. Rev. B* **2000**, *62*, 10000.
- (31) Grate, J. W. *Chem. Rev.* **2000**, *100*, 2627–2648.
- (32) Grate, J. W.; Abraham, M. H. *Sens. Actuators, B* **1991**, *3*, 85–111.
- (33) Grate, J. W. *Chem. Rev.* **2008**, *108*, 726–745.
- (34) Kolb, H. C.; Finn, M. G.; Sharpless, K. B. *Angew. Chem., Int. Ed.* **2001**, *40*, 2004–2021.
- (35) Dondoni, A. *Angew. Chem., Int. Ed.* **2008**, *47*, 8995–8997.
- (36) Chatterjee, A. K.; Choi, T.; Sanders, D. P.; Grubbs, R. H. *J. Am. Chem. Soc.* **2003**, *125*, 11360–11370.
- (37) Trnka, T. M.; Grubbs, R. H. *Acc. Chem. Res.* **2001**, *34*, 18–29.
- (38) Becer, C.; Hoogenboom, R.; Schubert, U. *Angew. Chem., Int. Ed.* **2009**, *48*, 4900–4908.
- (39) Osswald, S.; Havel, M.; Gogotsi, Y. *J. Raman Spectrosc.* **2007**, *38*, 728–736.
- (40) Amer, M. *Raman Spectroscopy, Fullerenes and Nanotechnology*; Royal Society of Chemistry: Cambridge, U.K., 2010.
- (41) Antunes, E.; Lobo, A.; Corat, E.; Trava-Airoldi, V.; Martin, A.; Verissimo, C. *Carbon* **2006**, *44*, 2202–2211.
- (42) Mennella, V.; Monaco, G.; Colangeli, L.; Bussoletti, E. *Carbon* **1995**, *33*, 115–121.
- (43) Crews, P.; Jaspars, M.; Rodríguez, J. *Organic Structure Analysis*; Oxford University Press: New York, 2009.
- (44) Jurs, P. C.; Bakken, G. A.; McClelland, H. E. *Chem. Rev.* **2000**, *100*, 2649–2678.
- (45) Kang, Y.; Rudkevich, D. M. *Tetrahedron* **2004**, *60*, 11219–11225.